Micro and nanofabrication of SiGe/Ge bridges and membranes by wet-anisotropic etching

V. Mondiali [a,c,*], M. Lodari [a], D. Chrastina [a], M. Barget [b], E. Bonera [b], M. Bollani [c]

[a] L-NESS, Dipartimento di Fisica, Politecnico di Milano, Polo di Como, via Anzani 42, I-22100 Como, Italy
[b] L-NESS and Dipartimento di Scienza dei Materiali, Università degli Studi Milano-Bicocca, via Cozzi 55, I-20125 Milano, Italy
[c] IFN-CNR, L-NESS, via Anzani 42, I-22100 Como, Italy

Received 29 October 2014
Received in revised form 7 March 2015
Accepted 24 March 2015
Available online 7 April 2015

1. Introduction

Information and communication technologies eagerly need novel approaches to continue the improvement of the performance and the scaling down of opto-electronic devices. Uniaxial strain obtained using local stressors has become part of mainstream Si-based technology, since uniaxial strain in Si improves its figures of merit [1,2]. The application of 4% uniaxial tensile strain along [1 0 0] to a Ge(0 0 1) layer is expected to lower the direct gap below the indirect gap [3,4]. A direct-gap semiconductor which is fully compatible with Si-based technology would suggest the possibility of highly efficient Si-compatible emitters of infrared radiation, which would greatly facilitate full integration of electronics and optoelectronics [5–7]. We have already demonstrated that top-down SiGe structures, fabricated by nanolithography, can be used as stressors for the creation of strong deformation fields and high strain in bulk substrates [8,9]. However, finite-element simulations suggest that a stressor patterned on a free-standing Ge membrane allows for a larger highly strained active area with respect to strained bulk material [10,11]. Therefore, the use of external stressors on Ge membranes instead of bulk substrates should be a very important step towards obtaining direct-gap Ge. This application is not part of the present work but is one of the possible extensions and a topic for future investigation.

Wet anisotropic etching is very useful in the fabrication of free-standing membranes, due to the high etch rate and low costs. This approach can provide a high selectivity in etching different materials, and even a noticeable crystallographic anisotropy. Typically wet etching is isotropic, but on crystalline materials, the etching rate of some etchants is lower on the more densely packed surfaces compared to the more loosely packed surfaces. Considering a diamond lattice structure, such as silicon, the surface atomic density is {1 1 1} > {1 0 0} > {1 1 0} and the etching rate (R) is about R(1 0 0) $\sim$ 100 $\times$ R(1 1 1) [12]. Recently, various etchants were also used in combination with atomic force microscopy (AFM) as a tool to investigate the composition of strained semiconductor islands (self-assembled quantum dots, QDs) or to reveal the morphology of QDs encapsulated in a semiconductor matrix. Based on the selectivity of the H_2O_2 solution, which etches $Si_{1-x}Ge_x$ alloys with x > 65% much more quickly than pure Si, Denker et al. [13] pro-vided evidence of the lateral composition profile in SiGe pyramids. Katsaros et al. [14] extended the previous approach to SiGe domes and suggested a kinetic model to account for the observed lateral profiles. In a more recent work, selective chemical etching and electron energy-loss spectroscopy are used to characterize the composition of Ge-rich islands [15]. On the contrary, to selectively etch Si, two alkaline solutions, potassium hydroxide (KOH) and tetramethylammonium hydroxide (TMAH), are normally used as

* Corresponding author. L-NESS, Dipartimento di Fisica, Politecnico di Milano, Polo di Como, via Anzani 42, I-22100 Como, Italy. Tel.: +39 0313327307.

E-mail address: valeria.mondiali@gmail.com (V. Mondiali).

etchants for anisotropic wet processes. The former has an excellent uniformity and reproducibility, but it is not compatible with MOS devices. To overcome this drawback, TMAH, already used in the development process in photolithography, was introduced as a solution for anisotropic wet etching. TMAH and KOH allow a high selectivity between etching rates in ⟨0 0 1⟩ and ⟨1 1 1⟩ directions in the silicon bulk [12]. For this reason they have been widely used in order to create suspended structures, for example by an etch against the etch-resistive {1 1 1} planes in Si(0 0 1) substrates [16,17] or by exploiting the underetching rates of a Si(0 0 1) substrate [18,19]. Germanium is extremely chemically resistive against KOH or TMAH [20,21], so it is potentially an excellent material for this kind of micromachining. Therefore, in this work a combination of lithographic process and dry and wet anisotropic etching has been used for the fabrication of both bridge and membranes which could be used to obtain a tensile strained material by a subsequent lithographic processes.

2. Material and methods

2.1. Material details

A 100 nm layer of Ge was deposited on a HF-dipped Si(0 0 1) 4-inch wafer by low-energy plasma-enhanced chemical vapor deposition (LEPECVD) at 500 °C and with a growth rate of 0.4 nm s^{-1}. Then, a tensile $Si_{1-x}Ge_x$ film ($0.6 \leqslant x \leqslant 0.9$; thickness ~ 10 nm) was grown on the Ge layer (Fig. 1(a)) at temperatures between 450 °C and 500 °C [22]. The SiGe capping layer could eventually be patterned by e-beam lithography into a stressor for the underlying Ge [10].

In addition, samples with no capping layer have been used: a Ge layer, 1 μm thick, was deposited at 500 °C and a growth rate of 4.3 nm s^{-1}, and then annealed in-situ over six cycles between 600 and 800 °C in order to reduce the threading dislocation density and to optimize the material quality.

2.2. Fabrication process

Prior to the wet etching experiments, we used photolithography or e-beam lithography (EBL) (Fig. 1(b) and (c)) and reactive ion etching (RIE) to define mesa structures on the sample surface. Optical lithography was used to fabricate membranes where the typical widths are between 10 and 20 μm (Fig. 1(b)). To realize bridges the EBL was used, in this case the typical widths are in the range between 0.1 and 3 μm, as shown in Fig. 1(c). In all cases, the Ge epitaxial film was etched by RIE, using a CF_4 plasma, 80 W RF power and total gas pressure of 54 mTorr.

Afterwards, in order to suspend the structure, the first series of samples were etched with TMAH (30% in vol.) at 85 °C and characterized by scanning electron microscopy (SEM) and μRaman. Instead, the second set of samples were etched with 5.3 wt% KOH (26.4 g KOH + 500 ml H_2O) at 70 °C. Two different geometries (bridges and membranes) have been realized using both etchants. For all the solutions both geometries have been fab-ricated, since different geometries (with different boundary condi-tions) can be used for different stressor configurations and applications [10]. The overall chemical etching reaction by alkaline solution is given by [23]:

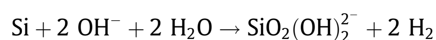

$$Si + 2\ OH^- + 2\ H_2O \rightarrow SiO_2(OH)_2^{2-} + 2\ H_2$$

Silicon reacts with water and an OH^- ion and produces hydroxide ions and hydrogen gas bubbles. The rate-limiting factor in KOH etching changes with the change of the concentration. So, at high concentration the chemical reaction that takes place on the Si surface limits the overall systems. On the other hand, at low concentration, the system is dominated by the diffusion of reacting species and reaction products. To prevent the adhesion of secondary products of the chemical reaction, such as SiO_x, the etching solution was kept in constant agitation. SiGe samples were etched at different times in order to infer the etch rate. Samples with different SiGe layers have been used in order to test the selectivity of the etchant solutions as a function of the Si fraction in the alloy. A representation of the obtained structures is reported in Fig. 1(d) and (e). All samples have been analyzed by μRaman to verify the presence of the SiGe film on top of the structures and by SEM in order to measure the etched thicknesses as shown in Fig. 1(f) and (g).

3. Results and discussion

The Si etching rate difference can be observed in Fig. 2(a) and (b), where the Si etched thicknesses are plotted as a function of the etching time. What is clear from these figures is the huge difference in the etch rate between TMAH and KOH [24–26]. The comparison between the respective results is shown in Fig. 2(c) and (d). Samples which show similar etched thickness are obtained after 50 min in TMAH and 1 min in KOH. In both cases the etching process does not begin immediately; this can be attrib-uted to the presence of a thin layer of silicon oxide, which is etched more slowly than Si [25]. In fact for KOH the SiO_2 etching rate is in the order of tens of nm/h and the Si etch rate is about tens of μm/h, while the TMAH solution shows slower SiO_2 as well as Si etching rates.

Using KOH etchant solution, the final surface quality points out some variations: in this case the (1 1 1) planes are very smooth and other stopping planes start to appear. The explanation can be found in the much higher R⟨1 0 0⟩/R⟨1 1 1⟩ selectivity (R) of KOH with respect to TMAH: the R⟨1 1 1⟩ is negligible if compared with the R⟨1 0 0⟩, which is hundreds of times faster. Whereas, when the concentration of the KOH solution is low, the rate along ⟨1 0 0⟩ is not the highest and different planes are etched faster. For instance, the ratio R⟨4 1 1⟩/R⟨1 0 0⟩ could be equal to 2 at low KOH concentration [26]. This brings out secondary Si crys-tallographic planes, leading to the creation of non square-shaped pyramidal bases for the membranes.

The etching rate changes with the concentration of KOH and with the temperature at which the process is performed. Higher temperatures and lower KOH concentrations lead to higher rates, which peak was obtained with a concentration of about 22% for a temperature of about 70 °C.

Fig. 3 shows the comparison between two different etching times in KOH, as can be noted from the different height and shape of the Si bases. For these samples, which have the same SiGe layer (Ge content ~ 60%), no significant differences occur for the SiGe/Ge membranes, in fact the surfaces are smooth with no porosity. Hence a high Si/Ge selectivity is provided by the KOH, yielding a gain in both etch rate and Si surface smoothness.

Finally, micro-Raman measurements have been performed in order to verify the selectivity of both solutions to Si and the preservation of the SiGe layer. The Raman spectra of both the unpatterned area and the bridge were measured using an excitation laser with a wavelength of 532 nm and a power of 0.06 mW focused with a 0.90 NA objective. With this excitation, the optical penetration depth is about 20 nm for Ge and SiGe. We performed the experiments with several excitation fluences in order to rule out heating effects due to the limited dissipation of heat by the suspended structures. The micro-Raman analyses were performed for all the samples with different SiGe layers and the results were similar. An example is shown in Fig. 4, where the two spectra are plotted, displaying an intense Ge peak and the small Ge-Ge and

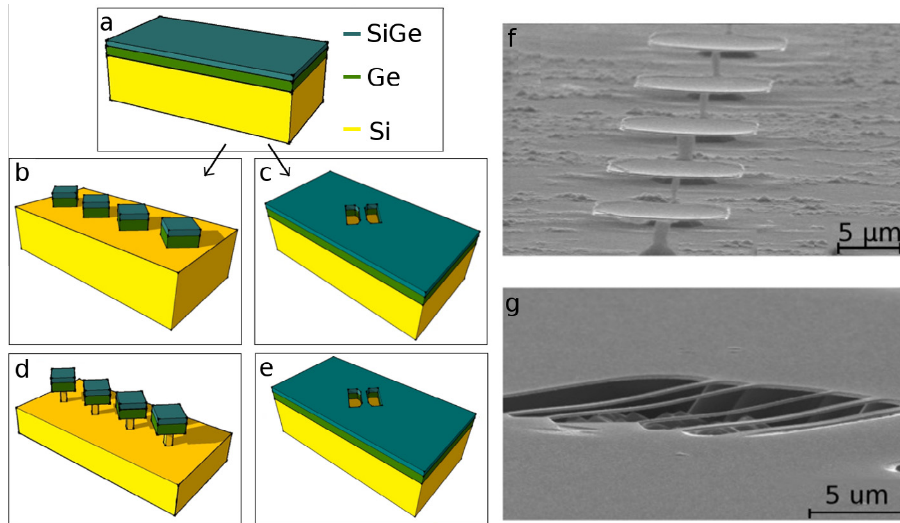

Fig. 1. (a)–(e) Schematic sequence of the fabrication steps for SiGe/Ge bridges and SiGe/Ge membranes on a Si(001) substrate, where the thicknesses and the size of nanostructures are not in scale. In (a) 100 nm of Ge and the SiGe capping layer (10 nm thick) are deposited by LEPECVD on a Si(001) substrate. The Ge content changes between 60% and 90%. (b) By optical lithography and RIE, a mask with squares or circles are defined. (c) By EBL and RIE, a mask with a bridge is defined. By wet chemical anisotropic etching, SiGe/Ge membranes (d) and bridges (e) are obtained. (f) SEM image of membranes 10 µm wide and 100 nm thick, etched with KOH. (g) SEM image of the bridges 0.3–1 µm wide, 10 µm long, and 100 nm thick, etched with TMAH. The bridges show bending because of strain relaxation of the initially slightly compressed Ge layer which results in an elongation of the bridge.

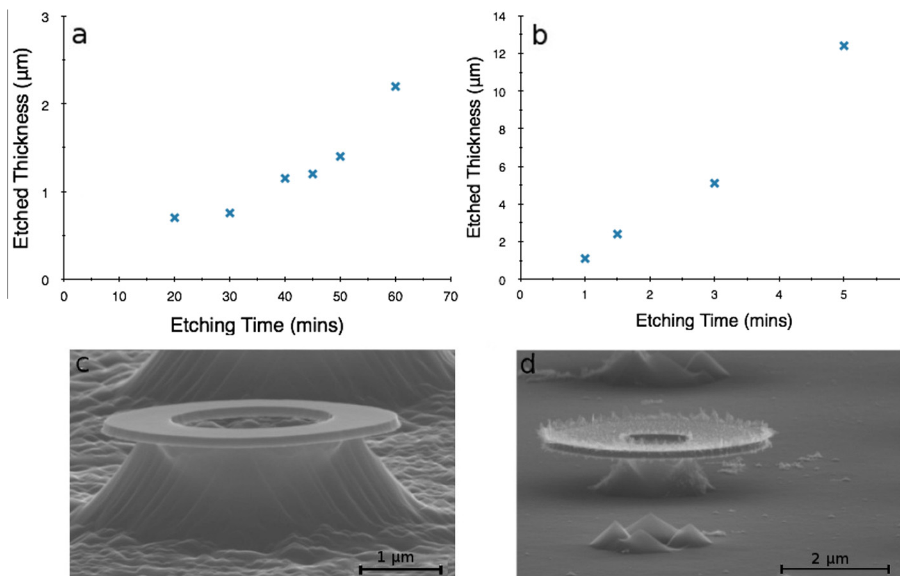

Fig. 2. Etched thickness as a function of the etching time, obtained using (a) TMAH and (b) KOH. The crosses show the experimental values, which are obtained by SEM images. (c) SEM image of the sample with a $Si_{0.1}Ge_{0.9}$ capping layer, after 50 min in TMAH at 85 °C. The etched thickness is about 1 µm. (d) SEM image of the sample with a $Si_{0.4}Ge_{0.6}$ capping layer, after 90 s in KOH at 70 °C. The etched thickness is about 1 µm.

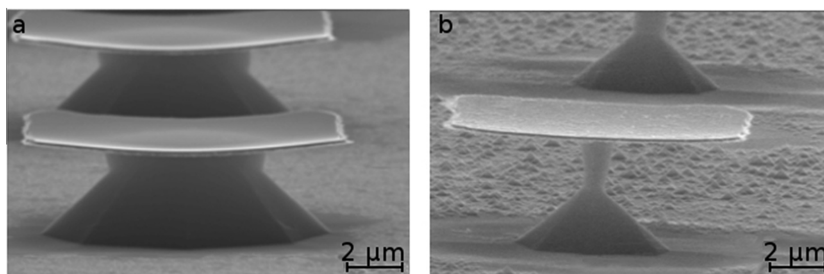

Fig. 3. (a) and (b) SEM images of different samples with the $Si_{0.4}Ge_{0.6}$ capping layer etched in KOH at 70 °C. (a) Sample etched for 90 s. (b) Sample etched for 3 min.

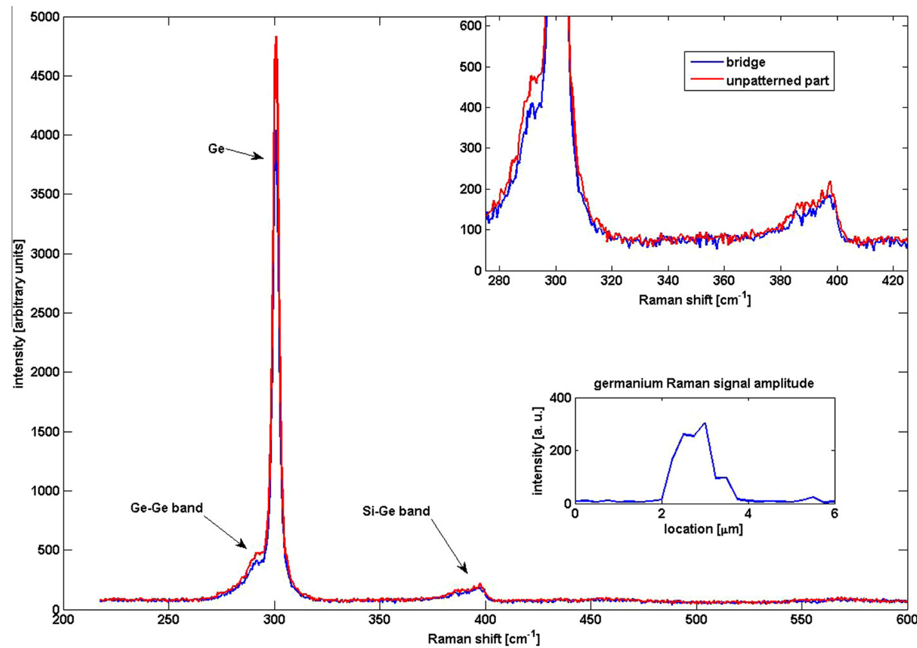

Fig. 4. Raman spectra of the sample with a Ge content of about 70% etched with KOH for 80 s. Both the spectrum of the unpatterned part and that of the bridge show the Raman bands for both Ge and SiGe. The upper inset shows an enlargement of the bands of both spectra. The lower inset shows the Ge Raman signal intensity of a line scan perpendicular to a bridge. Off the bridge the signal from Ge vanishes.

Si-Ge bands of the SiGe alloy. [27–29] Due to the low silicon content of the alloy, the Si-Si band of the SiGe is too low to be detected. The SiGe bands prove that the top layer is preserved in both cases. The unpatterned area and the bridge are in a very similar strain condition. We fitted the positions of the Ge peak and the Ge-Ge mode of the SiGe alloy. These are 300.7 ± 0.2 cm^{-1} and 290.1 ± 0.4 cm^{-1}, respectively, for the unpatterned area, and 300.8 ± 0.2 cm^{-1} and 290.6 ± 0.5 cm^{-1} for the bridge. These values are consistent with a slightly compressed germanium (−0.1 ± 0.1%) and a tensilely strained SiGe layer (composition 0.72 ± 0.01, strain 0.9 ± 0.1%). A SiGe layer coherent with a relaxed Ge would exhibit a strain of 1.2%. The measured Raman shift values hence indicate partial relaxation of SiGe. The very good agreement between the two spectra proves that both bridge and bulk have the same material composition, confirming the selectivity of the chemical solutions to etch only the pure silicon underneath the structures.

Investigation of the membranes by means of μRaman measurements were carried out using the same excitation laser as in the previous case, but with 0.25 mW excitation power. The germanium layer is found to be slightly compressed ($\varepsilon = -0.2\% \pm 0.1\%$) whereas the SiGe layer shows strain values between coherent growth and complete relaxation. Thus, SiGe is partially relaxed which is consistent with the observation from SEM images (Fig. 3) that the rim of the disk is slightly bent upwards to release strain in the SiGe layer. As previously stated, this result refers to a Ge layer below an un-patterned SiGe layer. Simulations (Ref. [10]) show that patterning of the strained SiGe layer should lead to transfer of strain to the Ge layer, forming regions in which the Ge is highly tensile.

4. Conclusions

In this work we have used KOH and TMAH, to realize bridge and membranes on a Si(001) substrate. With respect to TMAH, diluted KOH solutions can provide great improvement of the etch rate R, leading to a saving of time and resources, however TMAH allows a higher surface quality. The Si selectivity and the preservation of the SiGe capping layer, which is necessary to avoid the damage to the stressors, has been verified by micro-Raman measurements, which confirm that SiGe alloys are not aggressively attacked by the investigated etchant solutions. The capability to select pure Si material to be etched and not the Ge-rich SiGe alloy is essential to realize free-standing Ge structures for a new class of tensile Ge nano-substrates.

Acknowledgement

We acknowledge the Cariplo Foundation – Italy (within the grant DefCon4 2011-0331) for the financial support.

References

[1] R.A. Minamisawa, M.J. Süess, R. Spolenak, J. Faist, C. David, J. Gobrecht, K.K. Bourdelle, H. Sigg, Nat. Commun. 3 (2012) 1096, http://dx.doi.org/10.1038/ncomms2102.
[2] S.E. Thompson, G. Sun, K. Wu, J. Lim, T. Nishida, IEDM Tech. Dig. (2004) 221–224, http://dx.doi.org/10.1109/IEDM.2004.1419114.
[3] C. Boztug, J.R. Sánchez-Pérez, F.F. Sudradjat, R.B. Jacobson, D.M. Paskiewicz, M.G. Lagally, R. Paiella, Small 9 (2013) 622–630, http://dx.doi.org/10.1002/smll.201201090.
[4] P. Boucaud, M. El Kurdi, S. Sauvage, M. de Kersauson, A. Ghrib, X. Checoury, Nat. Photonics 7 (2013) 162, http://dx.doi.org/10.1038/nphoton.2013.12.
[5] M.J. Süess, R. Geiger, R.A. Minamisawa, G. Schiefler, J. Frigerio, D. Chrastina, G. Isella, R. Spolenak, J. Faist, H. Sigg, Nat. Photonics 7 (2013) 466–472, http://dx.doi.org/10.1038/nphoton.2013.67.
[6] J. Michel, J. Liu, L.C. Kimerling, Nat. Photon. 4 (2010) 527–534, http://dx.doi.org/10.1038/NPHOTON.2010.157.
[7] R. Soref, Nat. Photonics 4 (2010) 495–497, http://dx.doi.org/10.1038/nphoton.2010.171.
[8] M. Bollani, D. Chrastina, M. Fiocco, V. Mondiali, J. Frigerio, L. Gagliano, E. Bonera, J. Appl. Phys. 112 (2012) 094318, http://dx.doi.org/10.1063/1.4765009.
[9] E. Bonera, M. Bollani, D. Chrastina, F. Pezzoli, A. Picco, O.G. Schmidt, D. Terziotti, J. Appl. Phys. 113 (2013) 164308, http://dx.doi.org/10.1063/1.4802686.
[10] D. Scopece, F. Montalenti, M. Bollani, D. Chrastina, E. Bonera, Semicond. Sci. Technol. 29 (2014) 095012, http://dx.doi.org/10.1088/0268-1242/29/9/095012.
[11] D. Nam, D. Sukhdeo, A. Roy, K. Balram, S.L. Cheng, K.C.Y. Huang, Z. Yuan, M. Brongersma, Y. Nishi, D. Miller, K. Saraswat, Opt. Express 19 (2011) 25866, http://dx.doi.org/10.1364/OE.19.025866.
[12] M. Shikida, K. Sato, K. Tokoro, D. Uchikawa, Sens. Actuators A 73 (1999) 179–188, http://dx.doi.org/10.1016/S0924-4247(99)00264-2.
[13] U. Denker, M. Stoffel, O.G. Schmidt, Phys. Rev. Lett. 90 (2003) 196102, http://dx.doi.org/10.1103/PhysRevLett. 90.196102.

[14] G. Katsaros, G. Costantini, M. Stoffel, R. Esteban, A.M. Bittner, A. Rastelli, U. Denker, O.G. Schmidt, K. Kern, Phys. Rev. B 72 (2005) 195320, http://dx.doi.org/10.1103/PhysRevB.72.195320.

[15] M. Bollani, D. Chrastina, V. Montuori, D. Terziotti, E. Bonera, G.M. Vanacore, A. Tagliaferri, R. Sordan, C. Spinella, G. Nicotra, Nanotechnology 23 (2012) 045302, http://dx.doi.org/10.1088/0957-4484/23/4/045302.

[16] S.D. Rhead, J.E. Halpin, V.A. Shah, M. Myronov, D.H. Patchett, P.S. Allred, V. Kachkanov, I.P. Dolbnya, J.S. Reparaz, N.R. Wilson, C.M. Sotomayor Torres, D.R. Leadley, Appl. Phys. Lett. 104 (2014) 172107, http://dx.doi.org/10.1063/1.4874836.

[17] V.A. Shah, S. Rhead, J. Halpin, O. Trushkevych, E. Chávez-Ángel, M. Myronov, J.S. Reparaz, R. Edwards, F. Alzina, A. Shchepetov, S. Kachkanov, N.R. Wilson, I. Dolbnya, D.H. Patchett, P.S. Allred, M.J. Prest, P.M. Gammon, M. Prunnila, T.E. Whall, E.H.C. Parker, C.M. Sotomayor Torres, D.R. Leadley, J. Appl. Phys. 115 (2014) 144307, http://dx.doi.org/10.1063/1.4870807.

[18] A. Pandy, L.M. Landsberger, B. Nikpour, M. Paranjape, M. Kahrizi, J. Vac. Sci. Technol., A 16 (1998) 868, http://dx.doi.org/10.1116/1.581025.

[19] M. Paranjape, A. Pandy, S. Brida, L. Landsberger, M. Kahrizi, M. Zen, J. Vac. Sci. Technol., A 18 (2000) 738, http://dx.doi.org/10.1116/1.582169.

[20] B. Li, B. Xiong, L.N. Jiang, Y. Zohar, M. Wong, J. Microelectromech. Syst. 8 (1999) 366, http://dx.doi.org/10.1109/84.809050.

[21] V.A. Shah, M. Myronov, C. Wongwanitwatana, L. Bawden, M.J. Prest, J.S. Richardson-Bullock, S. Rhead, E.H.C. Parker, T.E. Whall, D.R. Leadley, Sci. Technol. Adv. Mater. 13 (2012) 055002, http://dx.doi.org/10.1088/1468-6996/13/5/055002.

[22] J. Frigerio, M. Lodari, D. Chrastina, V. Mondiali, G. Isella, M. Bollani, J. Appl. Phys. 116 (2014) 113507, http://dx.doi.org/10.1063/1.4896076.

[23] H. Seidel, L. Csepregi, A. Heuberger, H. Baumgärtel, J. Electrochem. Soc. 137 (1990) 3612–3626, http://dx.doi.org/10.1149/1.2086277.

[24] KOH etching of Silicon – Stanford Nanofabrication Facility (22-10-2014) <https://snf.stanford.edu/SNF/processes/process-modules/etching/wet-etching/si-wet-etching-at-snf/koh-etching-of-silicon>.

[25] KOH Etching of Silicon wafers, Silicon Dioxide (SiO_2) and Silicon Nitride (SiN) (22-10-2014) <http://www.cleanroom.byu.edu/KOH.phtml>.

[26] NCSU Nanofabrication Facility. Report on KOH Process Module. (22-10-2014) <http://www.nnf.ncsu.edu/sites/default/files/KOHReport_FINAL.pdf>.

[27] F. Pezzoli, L. Martinelli, E. Grilli, M. Guzzi, S. Sanguinetti, M. Bollani, D. Chrastina, G. Isella, H. von Känel, E. Wintersberger, J. Stangl, G. Bauer, Mater. Sci. Eng. B 124–125 (2005) 127–131, http://dx.doi.org/10.1016/j.mseb.2005.08.057.

[28] M.Z. Hossain, H.T. Johnson, J. Appl. Phys. 107 (2010) 073515, http://dx.doi.org/10.1063/1.3371678.

[29] A. Picco, E. Bonera, E. Grilli, M. Guzzi, M. Giarola, G. Mariotto, D. Chrastina, G. Isella, Phys. Rev. B 82 (2010) 115317, http://dx.doi.org/10.1103/PhysRevB.82.115317.